Annals of Nuclear Medicine (2020) 34:329–336
https://doi.org/10.1007/s12149-020-01452-z

ORIGINAL ARTICLE

Diagnosis of bladder cancer using ^{18}F-labeled α-methyl-phenylalanine tracers in a mouse model

Isa Mahendra[1,3] · Hirofumi Hanaoka[2] · Aiko Yamaguchi[2,4] · Tumenjargal Amartuvshin[1] · Yoshito Tsushima[1,5]

Received: 9 December 2019 / Accepted: 21 February 2020 / Published online: 6 March 2020

Abstract

Objective Although 2-^{18}F-fluoro-2-deoxy-glucose (^{18}F-FDG) has established roles in the diagnosis of a variety of cancers, it has limited value in the detection of primary/recurrent lesions in the bladder, mainly because of interference by the pooled radioactivity in the urine. Our previous study revealed promising properties of L- and D-2-^{18}F-α-methyl-phenylalanine (2-^{18}F-FAMP) as radiotracers; i.e., their rapid blood clearance and low renal accumulation. In the present study we evaluated the utility of L- and D-2-^{18}F-FAMP for imaging bladder cancer in a mouse model.

Methods We used the human bladder cancer cell line HT1376 to prepare a bladder cancer xenograft model in mice bearing both orthotopic and subcutaneous tumors. Biodistribution and PET imaging studies were performed at 1 and 3 h after injection of L-2-^{18}F-FAMP or D-2-^{18}F-FAMP. ^{18}F-FDG was used as a control.

Results At 1 h after injection, greater accumulations of both L-2-^{18}F-FAMP and D-2-^{18}F-FAMP were observed in the orthotopic tumors compared to ^{18}F-FDG. The orthotopic tumor-to-muscle ratio of D-2-^{18}F-FAMP was significantly higher than that of ^{18}F-FDG ($p < 0.01$), because of the rapid blood clearance of D-2-^{18}F-FAMP. L-2-^{18}F-FAMP showed the highest subcutaneous tumor-to-muscle ratio ($p < 0.01$) due to its high subcutaneous tumor uptake. Compared to L-2-^{18}F-FAMP, D-2-^{18}F-FAMP exhibited faster clearance and lower kidney accumulation. In the PET imaging studies, L- and D-2-^{18}F-FAMP both clearly visualized the orthotopic bladder tumors at 1 h after injection.

Conclusion Our study showed that L-2-^{18}F-FAMP and D-2-^{18}F-FAMP have the potential to detect bladder cancer.

Keywords Bladder cancer · PET imaging · F-18-labeled amino acid · Mouse model

Introduction

Bladder cancer is the tenth most common cancer worldwide [1]. At the time of diagnosis, 75% of bladder cancer patients have superficial tumors, and 25% present with muscle-invasive or metastatic disease that is associated with a high risk of death from distant metastases [2]. The extent of bladder wall infiltration has a role in the selection of treatment options for bladder cancer, and accurate staging is thus necessary to help guide patient management. The current gold standard for the diagnosis of bladder cancer is an invasive cystoscopy because the conventional noninvasive methods such as computed tomography (CT) and magnetic resonance imaging (MRI) that depend on morphologic information for diagnosis are insufficient [3–5].

In contrast to CT and MRI, positron emission tomography (PET) relies on functional information for diagnoses. The most commonly used PET tracer in oncological imaging is 2-^{18}F-fluoro-2-deoxy-glucose (^{18}F-FDG), which also has

✉ Hirofumi Hanaoka
hanaokah@gunma-u.ac.jp

1 Department of Diagnostic Radiology and Nuclear Medicine, Gunma University Graduate School of Medicine, 3-39-22 Showa, Maebashi 371-8511, Japan

2 Department of Bioimaging and Information Analysis, Gunma University Graduate School of Medicine, 3-39-22 Showa, Maebashi 371-8511, Japan

3 Center for Applied Nuclear Science and Technology, National Nuclear Energy Agency of Indonesia, Tamansari 71, Bandung, West Java 40132, Indonesia

4 Texas Therapeutics Institute, The Brown Foundation Institute of Molecular Medicine, The University of Texas Health Science Center at Houston, Houston, TX 77054, USA

5 Research Program for Diagnostic and Molecular Imaging, Division of Integrated Oncology Research, Gunma University Initiative for Advanced Research (GIAR), Gunma University Graduate School of Medicine, 3-39-22 Showa, Maebashi 371-8511, Japan

established roles in the initial staging, response assessment, and detection of the recurrence of many types of cancer [6]. However, the pooled radioactivity in the bladder derived from the urinary excreted ^{18}F-FDG hinders the detection of bladder cancer [3, 7]. The potential of other PET tracers such as ^{11}C-acetate, ^{11}C-choline, and ^{11}C-methionine for detecting bladder cancer has been investigated [3, 8], but the short half-life of ^{11}C (20 min) has restricted the wider application of these tracers.

Another type of promising radiotracer for cancer imaging is ^{18}F-labeled amino acid analogs targeting L-type amino acid transporter 1 (LAT1) [9, 10], which is overexpressed in various types of cancer including bladder cancer [11]. The relatively long half-life of ^{18}F (110 min) and its high tumor specificity make these tracers attractive. Regarding these tracers, we recently found that two isomers of the ^{18}F-labeled phenylalanine analog ^{18}F-fluoro-alpha-metylphenylalanine (^{18}F-FAMP) have an ideal property for bladder cancer imaging; i.e., the rapid elimination from the entire body including the kidneys and thus potentially eliminate the need for the cumbersome bladder irrigation [12]. We conducted the present study to evaluate the usefulness of two selected isomers of ^{18}F-FAMP (L-2-^{18}F-FAMP and D-2-^{18}F-FAMP) for imaging bladder cancer using a murine orthotopic and subcutaneous tumor xenograft model.

Materials and methods

Preparation of radiotracers

^{18}F-FDG, L-2-^{18}F-FAMP, and D-2-^{18}F-FAMP were produced at the biomedical cyclotron facility of Gunma University as described [12]. L- and D-2-^{18}F-FAMP were manually purified by reversed-phase HPLC and reconstituted in saline after the removal of the organic solvent. The radiochemical purity was > 95% for all three tracers. The specific activity of each ^{18}F-FAMP was 2–3 MBq/μmol.

Cellular uptake studies

Human bladder carcinoma cell line HT1376 was purchased from American Type Culture Collection (Manassas, VA). For the cellular uptake studies, cells (1×10^6 cells/well) were pre-incubated in the medium overnight in a 24-well culture plate. After incubation, the culture medium was removed, and the cells were washed with Na^+-free Hank's balanced salt solution (HBSS). The cells were then incubated with Na^+-free HBSS containing L- or D-2-^{18}F-FAMP (100 kBq) at 37 °C for 0, 10, 40, 70, and 120 min. After the incubation, cells were washed with Na^+-free HBSS and then lysed with 200 μL of 0.2 M NaOH. The radioactivity in the cell lysate was measured by a well-type γ-counter (ARC-7001; Hitachi-Aloka Medical, Tokyo). The radioactivity of each sample was normalized for the total protein concentration, which was determined using a Protein Assay kit (Modified Lowry Protein Assay Reagent; Pierce Chemical Co., Rockford, IL). For inhibition assay of cellular uptake, L- or D-2-^{18}F-FAMP (100 kBq) was incubated at 37 °C for 30 min in the presence of 10 or 100 μM of α-methyl-tyrosine. Then, the cellular uptake of each sample was analyzed as described above.

Animal model

All experimental protocols were approved by the Laboratory Animal Care and Use Committee of Gunma University.

We injected BALB/c nude mice (Japan SLC, Shizuoka, Japan) with 4×10^6 HT1376 cells suspended in 100 μL of a 1:1 mixture of PBS and Matrigel (Corning Life Sciences, Corning, NY) into the flank to obtain subcutaneous tumors. Four weeks after the subcutaneous implantation, orthotopic implantation was performed in the same animals as described [13–15] to establish both subcutaneous and orthotopic tumors of suitable sizes at the time of the experiment. The bladder of the mouse was exposed by a midline laparotomy under anesthesia with isoflurane. Then, 4×10^6 HT1376 cells suspended in 50 μL of the 1:1 PBS/Matrigel mixture were intramurally injected into the bladder wall of the mouse. The orthotopic tumor's growth was monitored for 3–4 weeks by bladder palpation.

Biodistribution studies

After the orthotopic and subcutaneous tumors had developed, the mice were subjected to biodistribution studies. A saline solution of L-2-^{18}F-FAMP, D-2-^{18}F-FAMP, or ^{18}F-FDG (0.2 MBq/100 μL) was injected into the tail vein of each mouse. At selected time points (1 and 3 h after the injection of L- or D-2-^{18}F-FAMP and 1 h after the injection of ^{18}F-FDG), mice were euthanized, and the organs of interest were dissected out and weighed. To minimize urine contamination, the bladder mucosa was washed with saline. The radioactivity of the collected samples was counted using a well-type γ-counter. The measurement results are expressed as the percentages of radioactivity per gram of organ (%ID/g).

PET imaging

PET imaging was performed using an animal PET scanner (Inveon; Siemens, Knoxville, TN). Approximately 2 MBq of L-2-^{18}F-FAMP or D-2-^{18}F-FAMP was injected into the tail vein of tumor-bearing mice. At 1 and 3 h after the injection, PET scans were acquired after euthanization and bladder wash using a catheter. After the whole-body imaging, tumor

and the tissues of interest were dissected out and ex vivo imaging was also performed.

For ^{18}F-FDG PET imaging, 2 MBq of the radiotracer was injected intravenously into the tumor-bearing mice under isoflurane anesthesia after the mice had been fasted overnight. The mice were kept under isoflurane anesthesia and the PET scans were performed at 1 h after injection as described above.

The acquisition time of each image was 10 min. The imaging data were reconstructed using an iterative OSEM3D/MAP procedure with the matrix size 128 × 128 × 159, including attenuation correction. The maximum intensity projection (MIP) images were displayed using AMIDE 1.0.4 software (Stanford University, Stanford, CA). The tumor-to-muscle ratio was calculated based on the %dose/mL of each organ, which was determined by placing the region of interest (ROI) on the whole organ of the ex vivo image with the use of an Inveon Research Workplace workstation (Siemens).

Immunohistochemistry

The expression of LAT1 in the fresh-frozen, O.C.T. compound (Sakura Finetek Japan, Tokyo)-embedded subcutaneous and orthotopic tumors was analyzed by immunohistochemical staining, which was carried out using an anti-LAT1 antibody (ab111106, Abcam, Cambridge, UK) and goat anti-rabbit IgG H&L (HRP) (ab6721, Abcam) followed by detection with DAKO Envision DAB substrate solution (Agilent Technologies, Santa Clara, CA). For a negative control, the primary antibody was replaced with PBS containing 0.1% bovine serum albumin.

Statistical analyses

The biodistribution study results are expressed as mean ± SD. The statistical analyses were performed using GraphPad Prism 8.2.0 software (GraphPad Software, La Jolla, CA). Differences between pairs of groups were analyzed using the unpaired *t*-test or one-way ANOVA with the Tukey multiple comparisons test where appropriate. Differences were accepted as significant when the *p* value was < 0.05.

Results

Cellular uptake studies

Both L-2-^{18}F-FAMP and D-2-^{18}F-FAMP were transported into HT1376 cell in a time-dependent manner (Fig. 1). L-2-^{18}F-FAMP showed a rapid uptake up to 10 min and reached the plateau, while the uptake of D-2-^{18}F-FAMP was gradually increased over time. As a result, the total uptake amount of D-2-^{18}F-FAMP became comparable to that of L-2-^{18}F-FAMP. The co-incubation of 100 μM of LAT1-specific inhibitor α-methyl-tyrosine significantly reduced the uptake of L- and D-2-^{18}F-FAMP to a similar extent (Fig. 1).

Biodistribution study

Figure 2 illustrates the radiotracer uptakes in the tumors and major organs at 1 h after injection. The L-2-^{18}F-FAMP uptake and the D-2-^{18}F-FAMP uptake in the tumors and organs of interest over time are summarized in Table 1. Reflecting rapid blood clearance, D-2-^{18}F-FAMP showed low accumulations in the non-target organs compared to L-2-^{18}F-FAMP ($p < 0.01$ in the blood and liver, $p < 0.05$ in the kidney and muscle). L- and D-2-^{18}F-FAMP showed high accumulation in the pancreas, which expresses LAT1 [16]. All three tracers showed accumulation in both the orthotopic and subcutaneous tumors (Fig. 2), and the expression of LAT1 was confirmed by the immunohistochemical analysis (Fig. 3). At 1 h after injection, the uptake of D-2-^{18}F-FAMP

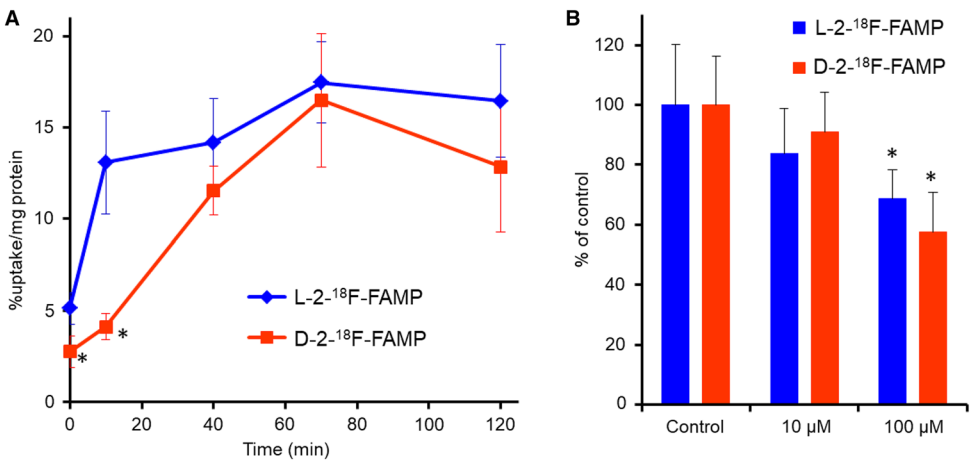

Fig. 1 **a** Cellular uptake of L-2-^{18}F-FAMP and D-2-^{18}F-FAMP by HT1376 cells at various time point ($n = 3$ or 4). A statistically significant difference from L-2-^{18}F-FAMP was indicated as $^*p < 0.05$. **b** Inhibition of cellular uptake of L-2-^{18}F-FAMP and D-2-^{18}F-FAMP in HT1376 cells by α-methyl-tyrosine ($n = 4$). A statistically significant difference from control was indicated as $^*p < 0.05$

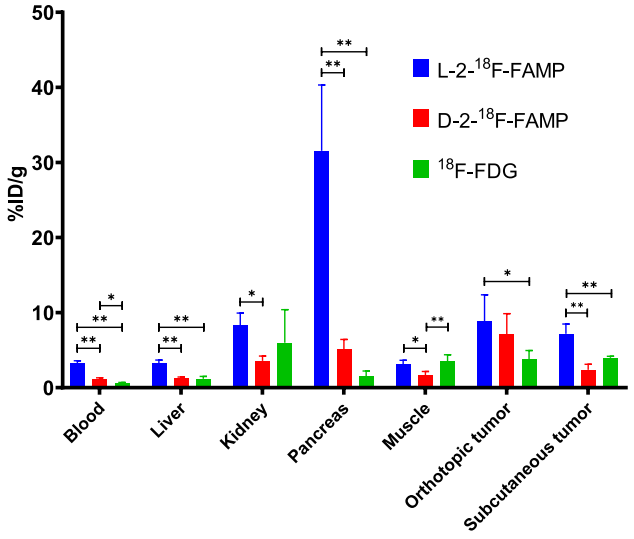

Fig. 2 Biodistribution of L-2-^{18}F-FAMP, D-2-^{18}F-FAMP, and ^{18}F-FDG in tumor-bearing mice at 1 h after injection ($n=4$ or 5). *$p<0.05$, **$p<0.01$

in the orthotopic tumors was significantly higher than that in the subcutaneous tumors ($p<0.01$). In contrast, the uptake levels of L-2-^{18}F-FAMP and ^{18}F-FDG were comparable between the orthotopic and subcutaneous tumors.

To further evaluate the tumor detectability of L- and D-2-^{18}F-FAMP, we compared the tumor-to-muscle, tumor-to-blood, and tumor-to-kidney ratios (Fig. 4). The orthotopic tumor-to-muscle ratio of D-2-^{18}F-FAMP was significantly higher than that of ^{18}F-FDG ($p<0.01$) due to its high orthotopic tumor uptake and low muscle uptake. L-2-^{18}F-FAMP showed the highest subcutaneous tumor-to-muscle ratio ($p<0.01$) due to its high subcutaneous tumor uptake. The subcutaneous tumor-to-blood ratios of L-2-^{18}F-FAMP and D-2-^{18}F-FAMP were lower than that of ^{18}F-FDG. In contrast, D-2-^{18}F-FAMP had an orthotopic tumor-to-blood ratio comparable to that of ^{18}F-FDG due to its high orthotopic tumor uptake and relatively fast blood clearance. There was no significant difference in the tumor-to-kidney ratio among the three tracers.

PET imaging studies

The PET imaging of L-2-^{18}F-FAMP, D-2-^{18}F-FAMP, and ^{18}F-FDG in the murine HT1376 xenograft model was performed at 1 h after each radiotracer's administration (Fig. 5). All three tracers clearly visualized the orthotopic tumors. In contrast, the subcutaneous tumors showed weak radiotracer uptakes. Following the whole-body imaging, ex vivo imaging was performed to quantify the tumor-to-muscle ratios. The orthotopic tumor-to-muscle ratios of all three tracers were higher than their subcutaneous tumor-to-muscle ratios. High uptakes of L-2-^{18}F-FAMP and D-2-^{18}F-FAMP were noted in the pancreas and kidney. ^{18}F-FDG showed high accumulations in the heart and kidney. PET imaging of L-2-^{18}F-FAMP and D-2-^{18}F-FAMP was also performed at 3 h after injection (Fig. 6); due to the fast elimination of these radiotracers from the body, the orthotopic tumors were more clearly visualized, resulting in increased tumor-to-muscle ratios.

Discussion

In the present study, we evaluated the utility of L- and D-2-^{18}F-FAMP for detecting bladder cancer using a LAT1-overexpressing bladder cancer xenograft model, and our results demonstrated that (1) L- and D-2-^{18}F-FAMP each showed high accumulation in the bladder tumors and rapid clearance from the body in the biodistribution study and (2) L- and

Table 1 Biodistribution of L-2-^{18}F-FAMP, D-2-^{18}F-FAMP, and ^{18}F-FDG in tumor-bearing mice

Organ	L-2-^{18}F-FAMP		D-2-^{18}F-FAMP		^{18}F-FDG
	1 h	3 h	1 h	3 h	1 h
Blood	3.27 ± 0.32	1.54 ± 0.62	1.12 ± 0.19	0.19 ± 0.02	0.60 ± 0.11
Liver	3.27 ± 0.42	1.54 ± 0.71	1.21 ± 0.21	0.21 ± 0.04	1.19 ± 0.31
Kidney	8.3 ± 1.64	3.95 ± 1.84	3.57 ± 0.64	0.57 ± 0.10	5.98 ± 4.40
Spleen	4.17 ± 0.50	1.89 ± 0.77	1.68 ± 0.33	0.25 ± 0.05	2.67 ± 0.63
Intestine	2.72 ± 0.30	1.26 ± 0.49	1.33 ± 0.22	0.76 ± 0.13	2.49 ± 0.53
Pancreas	31.5 ± 8.77	16.0 ± 7.20	5.09 ± 1.33	0.77 ± 0.15	1.49 ± 0.74
Lung	3.31 ± 0.44	1.52 ± 0.61	1.25 ± 0.24	0.20 + 0.04	3.02 ± 0.94
Heart	3.63 ± 0.35	1.76 ± 0.78	1.59 ± 0.28	0.30 ± 0.04	8.52 ± 5.75
Stomach	4.02 ± 1.80	1.56 ± 0.72	1.02 ± 0.26	0.23 ± 0.03	2.22 ± 1.14
Muscle	3.11 ± 0.54	2.59 ± 2.41	1.69 ± 0.46	0.51 ± 0.09	3.49 ± 0.90
Orthotopic tumor	8.89 ± 3.48	5.11 ± 3.26	7.12 ± 2.74	1.26 ± 0.77	3.75 ± 1.20
Subcutaneous tumor	7.17 ± 1.30	5.45 ± 1.84	2.38 ± 0.73	0.67 ± 0.05	3.98 ± 0.20

Each value is the mean percentage of the injected dose per gram of organ ± SD ($n=4$ or 5)

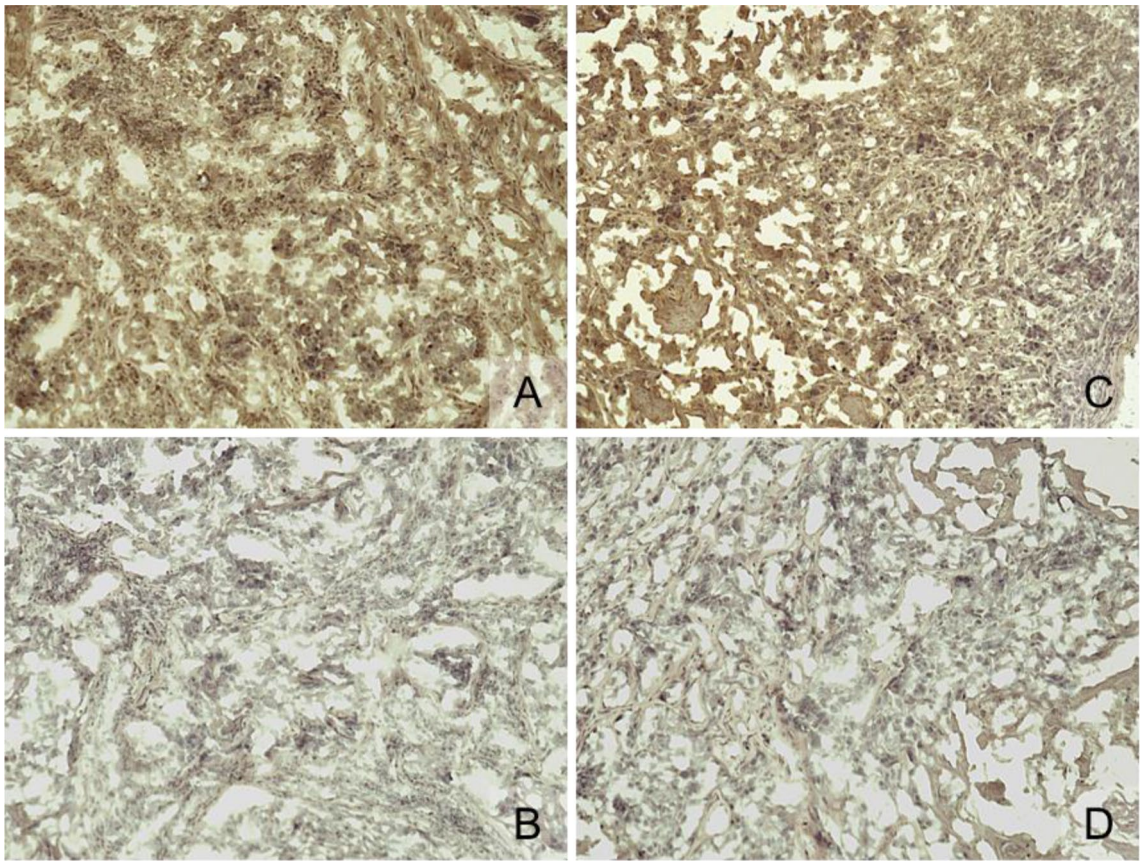

Fig. 3 Microscopy images (×10) of immunohistochemistry staining of LAT1 in HT1376 tumor. Orthotopic tumor samples with (**a**) or without (**b**) anti-LAT1 antibody, and subcutaneous tumors samples with (**c**) or without (**d**) anti-LAT1 antibody are shown

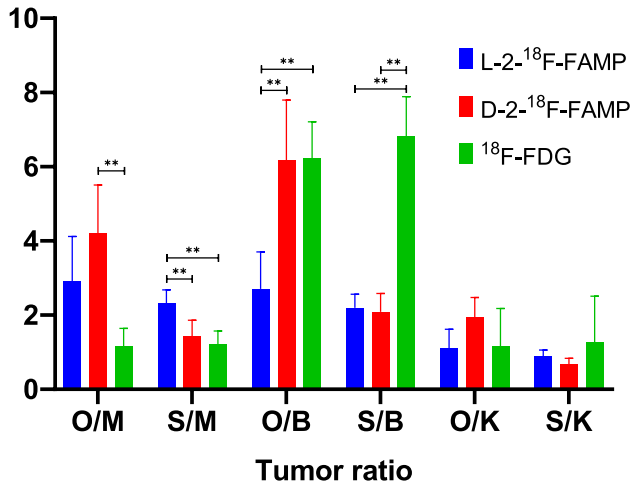

Fig. 4 Tumor-to-organ ratios of L-2-^{18}F-FAMP, D-2-^{18}F-FAMP, and ^{18}F-FDG in tumor-bearing mice at 1 h after injection ($n=4$ or 5). *B* blood, *K* kidney, *M* muscle, *O* orthotopic tumor, *S* subcutaneous tumor. *$p<0.05$, **$p<0.01$

D-2-^{18}F-FAMP each clearly visualized the tumors in the PET imaging. These results indicate the usefulness of both L- and D-2-^{18}F-FAMP for imaging bladder cancers.

An important issue that hampers the clinical use of ^{18}F-FDG-PET for the detection of bladder cancer is the necessity of bladder irrigation. Efforts have been made to improve the sensitivity of ^{18}F-FDG-PET using a furosemide injection or retrograde bladder irrigation [17, 18]; however, these techniques have provided only limited success in reducing intravesical activity because urine containing ^{18}F-FDG is excreted by kidneys and keeps trickling into the bladder. Although bladder irrigation was also necessary for the present study for L-2-^{18}F-FAMP and D-2-^{18}F-FAMP, we expect that the urinary radioactivity could be minimized in clinical settings by a simple urination control protocol. Since ^{18}F-FAMPs have rapid blood clearance and low renal accumulation [12], a continuous trickling of radioactivity into the bladder is unlikely after a certain time. Therefore, delayed postvoid scanning following natural diuresis (presumably several times) and oral hydration would be effective enough to minimize urine-derived radioactivity without decreasing the radiotracer's accumulation in the tumor. Although optimal time points and urination control protocol should be

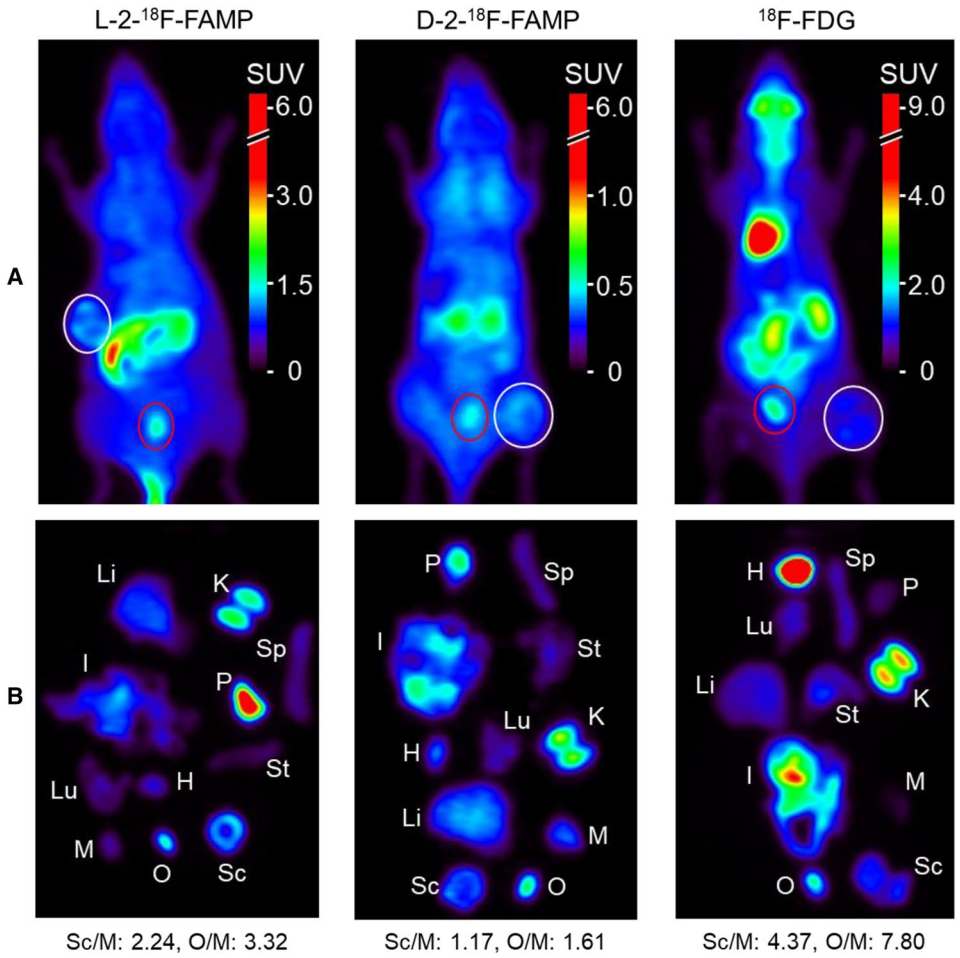

Fig. 5 **a** In vivo PET images of tumor-bearing mice with L-2-^{18}F-FAMP, D-2-^{18}F-FAMP, and ^{18}F-FDG at 1 h after injection ($n=1$). *Red circles* bladder with the tumor. *White circles* subcutaneous tumor. **b** Ex vivo PET images and tumor-to-muscle ratio at 1 h after injection ($n=1$). *H* heart, *I* intestine, *K* kidney, *Li* liver, *Lu* lung, *M* muscle, *O/M* orthotopic tumor-to-muscle ratio, *O* bladder with orthotopic tumor, *P* pancreas, *Sc/M* subcutaneous tumor-to-muscle ratio, *Sc* subcutaneous tumor, *Sp* spleen, *St* stomach

investigated in future clinical studies, our results support the conclusion that ^{18}F-FAMP could eliminate the necessity for bladder irrigation and thus could be a more convenient option for imaging bladder cancer compared to ^{18}F-FDG.

Since LAT1 takes up substrate amino acids in an obligatory exchange mechanism, the extracellular concentration of radiolabeled amino acids greatly impacts the tumor radiotracer accumulation levels. As such, the tumor accumulation level of radiolabeled amino acids gradually decreases in parallel with the radiotracer's blood clearance [12]. Radiolabeled alpha-methyl-phenylalanine analogs are almost exclusively excreted into the urine in their intact forms, which yields high radiotracer concentrations in the bladder [19]. We hypothesized that this increased extracellular concentration of L- or D-2-^{18}F-FAMP in the urine can be harnessed to facilitate the bladder tumor uptake of L- and D-2-^{18}F-FAMP via an intravesical drug delivery mechanism [20].

As expected, D-2-^{18}F-FAMP showed dramatically high orthotopic tumor uptake despite its subtle uptake in the subcutaneous tumors. It was reported that the L-form of ^{18}F-labeled alpha-methyl-tyrosine (^{18}F-FAMT), another LAT1 radiotracer, had rapid tumor cell uptake kinetics and reached a plateau after a 10-min incubation in vitro, whereas its D-form had slow tumor cell uptake kinetics and accumulated to a lesser extent [21]. D-2-^{18}F-FAMP also showed delayed uptake kinetics, however, its total accumulation was comparable to that of L-2-^{18}F-FAMP. We, therefore, speculate that the increased D-2-^{18}F-FAMP concentration in the urine and the extended contact with the tumor cells in the present study contributed to the increase in the tumor uptake levels of D-2-^{18}F-FAMP. In contrast, L-2-^{18}F-FAMP showed comparable uptake levels in subcutaneous and orthotopic tumors. We suspect that L-2-^{18}F-FAMP accumulated at the maximum levels in both tumors because of its rapid tumor uptake kinetics and relatively slow blood clearance. Although the absolute uptakes of L-2-^{18}F-FAMP and D-2-^{18}F-FAMP in the orthotopic tumors were comparable, D-2-^{18}F-FAMP showed a better tumor-to-blood ratio due to its fast blood clearance. Collectively, these results suggest that an intravesical pathway is a suitable drug delivery mechanism to facilitate the tumor uptake of D-2-^{18}F-FAMP.

In agreement with the biodistribution study, all three tracers clearly visualized tumors in the PET imaging study. D-2-^{18}F-FAMP showed that an orthotopic tumor-to-muscle ratio

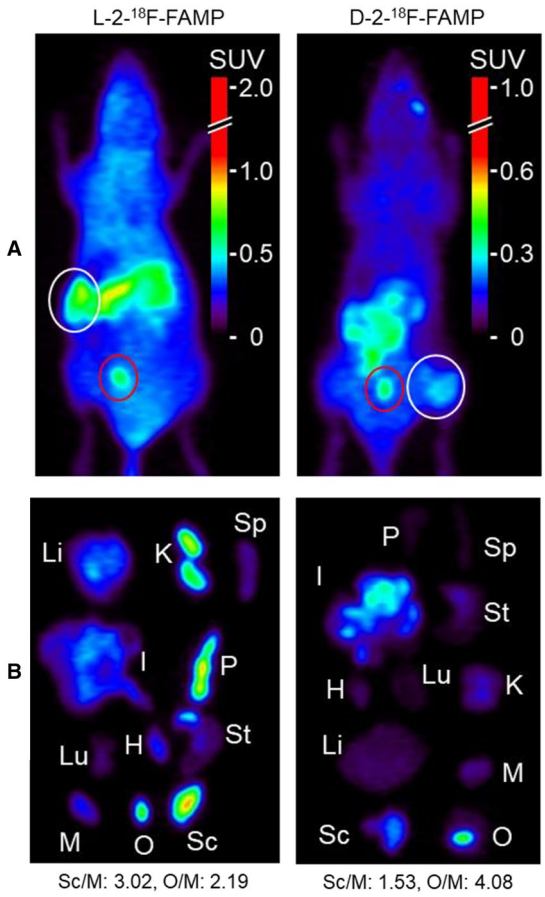

Fig. 6 **a** In vivo PET images of a tumor-bearing mouse with L-2-^{18}F-FAMP and D-2-^{18}F-FAMP at 3 h after injection ($n=1$). *Red circles* bladder with the tumor. *White circles* subcutaneous tumor. **b** Ex vivo PET images and the tumor-to-muscle ratio at 3 h after injection ($n=1$). *H* heart, *I* intestine, *K* kidney, *Li* liver, *Lu* lung, *M* muscle, *O/M* orthotopic tumor-to-muscle ratio, *O* bladder with orthotopic tumor, *P* pancreas, *Sc/M* subcutaneous tumor-to-muscle ratio, *Sc* subcutaneous tumor, *Sp* spleen, *St* stomach

in the PET imaging study was lower than that in the biodistribution study. A possible reason for this difference might be the high activity dose used in the PET imaging, which increased the total amount of substrate amino acids. Indeed, Ohshima et al. showed that a co-injection of a LAT1 substrate amino acid analog decreased the tumor-to-background contrast of D-^{18}F-FAMT by delaying blood clearance [21]. In addition to the increase in the background signal, the delayed blood clearance may also affect uptake of D-2-^{18}F-FAMP in the orthotopic tumor by delaying the inflow of radioactivity into the bladder. However, we observed that at 3 h after injection, the majority of the L-2-^{18}F-FAMP and D-2-^{18}F-FAMP was eliminated from the body, resulting in a clear visualization of both the orthotopic and subcutaneous tumors. These results indicate that delayed PET scanning would help to achieve the clear delineation of bladder cancers by L-2-^{18}F-FAMP and D-2-^{18}F-FAMP.

We took delayed images at 3 h after the radiotracer injections because L- and D-2-^{18}F-FAMP both showed retarded whole-body clearance compared to the results of a study examining a subcutaneous tumor xenograft mice model [12]. The high orthotopic tumor burden relative to the size of the murine bladder might have caused urination impairment and led to the increased retentions of L- and D-2-^{18}F-FAMP. Considering the clinical situation, high tumor-to-background contrast can be achieved at an earlier time point, because urination disorders are not frequent and the rapid clearance of ^{18}F-FAMPs is expected.

Conclusion

L-2-^{18}F-FAMP and D-2-^{18}F-FAMP showed high uptake in orthotopic bladder tumors and low accumulation in non-target organs. PET imaging with L-2-^{18}F-FAMP and D-2-^{18}F-FAMP clearly visualized the orthotopic bladder tumors. These results suggest the potential usefulness of the 2-^{18}F-FAMPs as radiotracers to detect bladder cancer.

Acknowledgements We thank Mr. Takashi Ogasawara (Cyclotron Facility, Gunma University Hospital) for producing the ^{18}F-FAMPs and ^{18}F-FDG. No potential conflicts of interest were disclosed.

References

1. Bray F, Ferlay J, Soerjomataram I, Siegel RL, Torre LA, Jemal A. Global cancer statistics 2018: GLOBOCAN estimates of incidence and mortality worldwide for 36 cancers in 185 countries. CA Cancer J Clin. 2018;68:394–424.
2. Kamat AM, Hahn NM, Efstathiou JA, Lerner SP, Malmström P-U, Choi W, et al. Bladder cancer. Lancet. 2016;388:2796–810.
3. Totaro A, Pinto F, Brescia A, Racioppi M, Cappa E, D'Agostino D, et al. Imaging in bladder cancer: present role and future perspectives. Urol Int. 2010;85:373–80.
4. Choe J, Braschi-Amirfarzan M, Tirumani SH, Shinagare AB, Kim KW, Ramaiya NH, et al. Updates for the radiologist in non-muscle-invasive, muscle-invasive, and metastatic bladder cancer. Abdom Radiol. 2017;42:2710–24.
5. Alfred Witjes J, Lebret T, Compérat EM, Cowan NC, De Santis M, Bruins HM, et al. Updated 2016 EAU guidelines on muscle-invasive and metastatic bladder cancer. Eur Urol. 2017;71:462–75.
6. Avril N. GLUT1 expression in tissue and ^{18}F-FDG uptake. J Nucl Med. 2004;45:930–3.
7. Razik A, Das C, Sharma S. PET-CT and PET-MR in urological cancers other than prostate cancer: an update on state of the art. Indian J Urol. 2018;34:20.
8. Schöder H, Larson SM. Positron emission tomography for prostate, bladder, and renal cancer. Semin Nucl Med. 2004;34:274–92.
9. Achmad A, Bhattarai A, Yudistiro R, Heryanto YD, Higuchi T, Tsushima Y. The diagnostic performance of ^{18}F-FAMT PET and ^{18}F-FDG PET for malignancy detection: a meta-analysis. BMC Med Imaging. 2017;17:66.
10. Watabe T, Ikeda H, Nagamori S, Wiriyasermkul P, Tanaka Y, Naka S, et al. ^{18}F-FBPA as a tumor-specific probe of L-type amino acid transporter 1 (LAT1): a comparison study with

^{18}F-FDG and ^{11}C-Methionine PET. Eur J Nucl Med Mol Imaging. 2017;44:321–31.
11. Maimaiti M, Sakamoto S, Sugiura M, Xu M, Yamada Y, Higuchi K, et al. An L-type amino acid transporte 1 inhibitor: JPH203 suppresses bladder cancer growth and invansion via IGFBP-5. J Urol. 2019;201:e724.
12. Hanaoka H, Ohshima Y, Yamaguchi A, Suzuki H, Ishioka NS, Higuchi T, et al. Novel ^{18}F-labeled α-methyl-phenylalanine derivative with high tumor accumulation and ideal pharmacokinetics for tumor-specific imaging. Mol Pharm. 2019;16:3609–16.
13. Ferreira-Teixeira M, Parada B, Rodrigues-Santos P, Alves V, Ramalho JS, Caramelo F, et al. Functional and molecular characterization of cancer stem-like cells in bladder cancer: a potential signature for muscle-invasive tumors. Oncotarget. 2015;6:36185–201.
14. Fu C-L, Apelo CA, Torres B, Thai KH, Hsieh MH. Mouse bladder wall injection. J Vis Exp. 2011;53:1–3.
15. Jäger W, Moskalev I, Janssen C, Hayashi T, Awrey S, Gust KM, et al. Ultrasound-guided intramural inoculation of orthotopic bladder cancer xenografts: a novel high-precision approach. PLoS ONE. 2013;8:e59536.
16. Abbas A, Beamish C, McGirr R, Demarco J, Cockburn N, Krokowski D, et al. Characterization of 5-(2–^{18}F-fluoroethoxy)-L-tryptophan for PET imaging of the pancreas. F1000Research. 2016;5:1851.
17. Nijjar S, Patterson J, Ducharme J, Leslie WD, Demeter SJ. The effect of furosemide dose timing on bladder activity in oncology imaging with ^{18}F-fluorodeoxyglucose PET/CT. Nucl Med Commun. 2010;31:167–72.
18. Anjos DA, Etchebehere ECSC, Ramos CD, Santos AO, Albertotti C, Camargo EE. ^{18}F-FDG PET/CT delayed images after diuretic for restaging invasive bladder cancer. J Nucl Med. 2007;48:764–70.
19. Hanaoka H, Ohshima Y, Suzuki Y, Yamaguchi A, Watanabe S, Uehara T, et al. Development of a widely usable amino acid tracer: ^{76}Br-α-methyl-phenylalanine for tumor PET imaging. J Nucl Med. 2015;56:791–7.
20. GuhaSarkar S, Banerjee R. Intravesical drug delivery: challenges, current status, opportunities and novel strategies. J Control Release. 2010;148:147–59.
21. Ohshima Y, Hanaoka H, Tominaga H, Kanai Y, Kaira K, Yamaguchi A, et al. Biological evaluation of 3-[^{18}F]fluoro-α-methyl-d-tyrosine (D-[^{18}F]FAMT) as a novel amino acid tracer for positron emission tomography. Ann Nucl Med. 2013;27:314–24.